PAPER *Special Section on Emerging Communication Technologies in Conjunction with Main Topics of ICETC2020*

# The Effect of Multi-Directional on Remote Heart Rate Measurement Using PA-LI Joint ICEEMDAN Method with mm-Wave FMCW Radar

**Yaokun HU**[†*a)] ***and*** **Takeshi TODA**[††]**,** ***Members***

**SUMMARY** Heart rate measurement for mm-wave FMCW radar based on phase analysis comprises a variety of noise. Furthermore, because the breathing and heart frequencies are so close, the harmonic of the breathing signal interferes with the heart rate, and the band-pass filter cannot solve it. On the other hand, because heart rates vary from person to person, it is difficult to choose the basic function of WT (Wavelet Transform). To solve the aforementioned difficulties, we consider performing time-frequency domain analysis on human skin surface displacement data. The PA-LI (Phase Accumulation-Linear Interpolation) joint ICEEMDAN (Improved Complete Ensemble Empirical Mode Decomposition with Adaptive Noise) approach is proposed in this paper, which effectively enhances the signal's SNR, estimates the heart rate, and reconstructs the heartbeat signal. The experimental findings demonstrate that the proposed method can not only extract heartbeat signals with high SNR from the front direction, but it can also detect heart rate from other directions (e.g., back, left, oblique front, and ceiling).

***key words:*** *FMCW radar, health care, heart rate, radar signal processing, vital signs*

## 1. Introduction

During the COVID-19 epidemic, the terms "remote" and "non-contact" have grown popular. Non-contact measuring devices have also become a pressing need in medical monitoring. Radar-based non-contact vital sign monitoring is unaffected by inclement weather or low light levels. As a result, it is widely used in domains such as medical monitoring and disaster relief. The research on the remote heart rate measuring system has progressed as radar technology has advanced in recent years.

To measure heartbeat with great precision, the authors of the research [1] employed Doppler radar based on the time-window-variation technique. T. Sakamoto et al. suggested an X-band array radar with an adaptive array processing technique for measuring a person's heart rate while several people in the scene in 2018 [2]. For ultra-wideband (UWB) radar, a vital sign extraction approach based on permutation entropy and the ensemble empirical mode decomposition (EEMD) algorithm was suggested [3]. Continuous-wave (CW) Doppler radars [1], [4]–[9] and impulse-radio ultra-wideband (IR-UWB) radars [3], [10]–[12] are two of the most regularly utilized radar techniques for non-contact vital sign monitoring. On the one hand, CW Doppler radars use a single-tone continuous-wave to collect phase history and provide a high degree of precision in displacement measurement. However, CW Doppler radars lack range capacity [13]. This implies that CW Doppler radars are subject to interference from moving objects and other clutter in the environment. Furthermore, in practice application, these effects cannot be disregarded. IR-UWB radars, on the other hand, may achieve excellent range resolution by transmitting with a huge bandwidth. And this is accomplished through the emission of very temporarily narrow radio impulses. Therefore, signal-energy levels that can be transmitted are not extremely high, lowering the accuracy and SNR (Signal-to-Noise Ratio) of IR-UWB radars [14]. Comparing with CW Doppler radars and IR-UWB radars, frequency-modulated continuous-wave (FMCW) radar does not only has the high sensitivity of CW Doppler radars but also has the ranging capability of impulse UWB radars. Furthermore, the wavelength of a 77 GHz FMCW radar is around 4 mm, and a minor movement might result in a substantial phase change of the IF signal. Therefore, this radar is used in this study to attain great range accuracy.

Although the range-bin selection and the IF signal phase analysis can accurately measure the radar vital sign (human vital signs detected by the radar), it still includes the body shaking of the subject and interference from other objects within the same range-bin besides the subject's respiratory and heartbeat signals. A band-pass filter (BPF) is a common way for separating the respiratory and heartbeat signals from the radar vital sign. However, the frequency of breathing and heart rate are very close, the heart rate is interfered with by the harmonic of the respiratory signal, and it cannot be solved by BPF [15]. The authors of [16], [17], on the other hand, employed wavelet transform (WT) to extract the heartbeat signal, but the heart rate varies from person to person, making the basic function of WT difficult to pick.

We consider performing time-frequency domain analysis on the radar vital sign to resolve the aforementioned concerns. Empirical mode decomposition (EMD) was proposed by Huang N.E. et al. in 1998, which is an adaptive signal processing method to analyze nonlinear and non-stationary signals [18]. In [3], [12], [19], they employed EMD or EEMD

Manuscript received February 24, 2021.
Manuscript revised June 8, 2021.
Manuscript publicized August 2, 2021.

[†]The author is with Graduate School of Science and Technology, Nihon University, Tokyo, 101-0062 Japan.
[††]The author is with College of Science and Technology, Nihon University, Tokyo, 101-0062 Japan.
[*]Presently, with Fujitsu Ltd., Japan.
a) E-mail: csgy19014@g.nihon-u.ac.jp

DOI: 10.1587/transcom.2021CEP0014

to measure heart rate using radar. Nonetheless, the EMD method is constrained by the phenomena of "mode mixing." EEMD [20] was presented as an improved EMD approach that resolves the problem by adding white Gaussian noise. However, EEMD has one major flaw: the decomposed signal contains residual noise. The issues discussed above might lead to instability in heart rate estimates. M.E. Torres et al. presented the complete ensemble empirical mode decomposition with adaptive noise (CEEMDAN) in 2011 [21]. By including adaptive white noise throughout each decomposition stage, this technique can eliminate the residual noise issue. Despite that, CEEMDAN still has some shortcomings, such as the signal information appears "later" than in EEMD with some "spurious" modes in the early stages of the decomposition. Three years later, an improved complete ensemble empirical mode decomposition with adaptive noise (ICEEMDAN) method was presented in [22]. This method can handle the problem of "mode mixing" without producing "spurious" modes and the residual noise. Therefore, we applied the ICEEMDAN method to perform time-frequency domain analysis on the radar vital sign [23]. However, because the heart intrinsic mode function (IMF) decomposed using the conventional ICEEMDAN method does not always have a high SNR, finding the peak and estimating the heart rate might be problematic.

Prior to time-frequency domain analysis, we presented a phase accumulation-linear interpolation (PA-LI) processing for FMCW radar signals. This approach can boost the SNR of the original signal fast and effectively, making it easier to detect the peak value of the heart IMF spectrum. In addition, the PA-LI technique's validity was established in combination with the EEMD method [24].

According to the advantages of the ICEEMDAN method and the PA-LI method discussed above. This will be the first paper to employ the PA-LI joint ICEEMDAN method to estimate the heart rate.

In terms of experimentation, most studies, such as paper [25], [26], had their subjects lying on the bed or sitting in a chair, and they monitored the heart rate solely from the front of the item. The authors of [27]–[29] took measurements from multiple horizontal directions (e.g., front, back, left, and right). In [30], T. Sakamoto et al. measured the heart rate from the top of the head. In this study, we will utilize the suggested measurement technique to estimate heart rate from multiple directions, assess the influence of different directions on the accuracy, and illustrate the validity and usefulness of the suggested approach.

## 2. FMCW Radar Principle for Heart Rate Estimation

Figure 1 shows a schematic representation of the FMCW radar-based vital signs measurement. The transmitted and received chirp signals of an FMCW radar in the frequency domain are shown in Fig. 2. Combining the above two figures shows that the ramp generator periodically outputs a chirp signal whose frequency increases linearly with time. Each chirp signal's frequency is swept linearly from $f_{\min}$ to $f_{\max}$

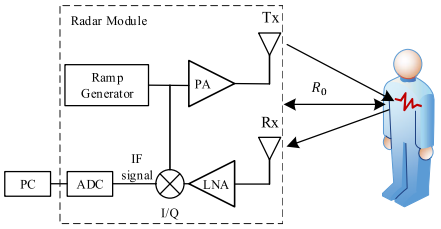


**Fig. 1** Block diagram of the FMCW radar, signal processing is performed in a PC using MATLAB 2018b. PA of this figure and LNA are the power amplifier and the low-noise amplifier, ADC means the analog-to-digital converter. Tx and Rx are abbreviations for transmit and receive, respectively.

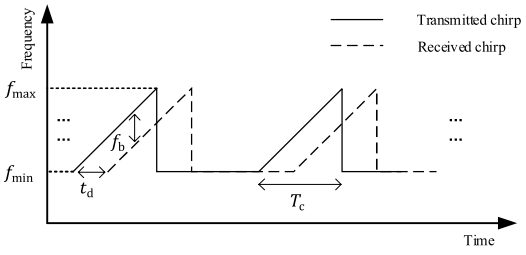


**Fig. 2** Transmitted chirp and received chirp of FMCW radar.

inside $T_c$, with a slope of $K_s$. Therefore, the chirp signal's sweeping bandwidth can be described as $B = f_{\max} - f_{\min} = K_s T_c$.

The power amplifier amplifies the transmit chirp signal. The amplified signal will then be transmitted via the transmitter antenna. The received chirp signal is amplified by the low-noise amplifier (LNA) and correlated with the transmit signal via the I/Q (In-phase and Quadrature) mixer, which produces the IF signal. The in-phase and quadrature components of the IF signal are then sampled separately to generate the received complex signal to preserve its phase information, subsequently processed in a PC (i7-9700 CPU 3 GHz). The instantaneous frequency difference can be used to calculate the subject's distance from the radar.

In terms of mathematical formulas, the radar transmitted chirp signal is stated as follows:

$$s_t(t) = A_t \exp\left(j\left(2\pi f_{\min} t + \pi K_s t^2\right)\right), 0 < t < T_c, \quad (1)$$

where $A_t$ denotes the magnitude related to the transmit power and $f_{\min}$ denotes the start frequency of the chirp. The transmitted signal is reflected on the subject and received with a time delay $t_d$ and $R_0$ represents the distance between the radar and the subject. The relationship between $t_d$ and $R_0$ is shown in Eq. (2).

$$t_d = \frac{2R_0}{c}, \quad (2)$$

where c represents the speed of light. The received chirp signal is $s_r(t) = A_r s_t(t - t_d)$, where $A_r$ has a relationship to $A_t$ by radar equation. To summarize, the IF signal is defined by the equation below.

$$s_{if}(t) = A_t A_r \exp\left(j\left(2\pi f_{\min} t_d + 2\pi K_s t_d t - \pi K_s t_d^2\right)\right)$$

$$\approx A_t A_r \exp\left(j\left(2\pi f_{\min} t_d + 2\pi K_s t_d t\right)\right), t_d < t < T_c, \quad (3)$$

where $\pi K_s t_d^2$ in Eq. (3) can be omitted because it is tiny. By substituting Eq. (2) into Eq. (3), we can obtain the frequency and phase of the IF signal, which can be expressed as follows.

$$f_b = \frac{2K_s R_0}{c}, \quad \varphi(t) = 4\pi f_{\min} \frac{(R_0 + x(t))}{c}, \quad (4)$$

where $R_0$ represents the instantaneous distance between the subject and the radar, and $x(t)$ represents the chest movement (radar vital sign) induced by breathing and heartbeat.

## 3. Proposed Method

The proposed method of vital signs monitoring is shown in Fig. 3. This study assumes that each IF signal (received complex signal) is sampled $m$ points by the ADC, and the total number of chirps for the whole measurement period is $n_{\text{chirp}}$. Following ADC sampling, we perform the Range-FFT computation on the received complex matrix ($[m, n_{\text{chirp}}]$) along the fast-time dimension to get a range profile matrix (RPM), which comprises subject's distance information. The surface weak vibration of the subject may then be detected by extracting the phase of the range-bin in which the subject is placed. However, the DC term of the received complex signal is created by leakage from Tx to Rx, which interferes with the phase quality [31]. This indicates that the phase $\varphi'(t)$ extracted from the received complex signal is not equal to the phase $\varphi(t)$ in Eq. (4), and their connection is shown as follows:

$$\varphi'(t) = \arctan\left(\frac{I(t) + dc_i}{R(t) + dc_r}\right) \neq \varphi(t), \quad (5)$$

where $R(t)$, $I(t)$, $dc_i$, and $dc_r$ are the real part, the imaginary part, the DC term of the imaginary part, and the DC term of the real part of the received complex signal. To eliminate the DC term, we utilize nonlinear least squares (NLLS) to estimate the center of the discrete data on the received complex signal's constellation diagram and then move the center to the origin.

Next, the collected phase information is subjected to phase accumulation-linear interpolation (PA-LI) processing to reduce phase noise and increase the SNR of radar vital sign $x(t)$ [24]. Generally, measured phase change due to the chest movement is very slow, and heart rate is 0.8–2.0 Hz under normal conditions. Therefore, in most studies, such as [25], [26], there is only one chirp in one frame, and the frame period is generally set at 50–100 ms according to the Nyquist-Shannon sampling theorem, corresponding to a sampling rate of 10–20 Hz (5–10 times the usual maximum heart rate). However, in the scenario, the time utilization is very poor due to the excessive idle time between frames. Besides, the phase analysis processes under highly non-linearity. Therefore, we proposed transmitting multiple chirps in each frame period and then accumulating all received signals in a single frame period to eliminate phase noise, called phase accumulation (PA) [24].

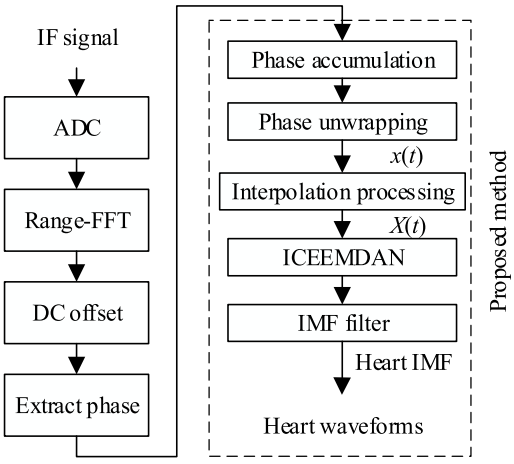


**Fig. 3** Flow chart of the proposed signal processing.

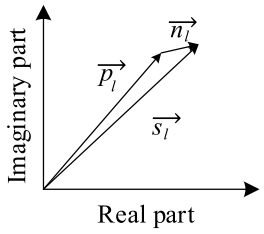


**Fig. 4** Phase diagram of the received signal.

The phase diagram of the range-bin in which the subject is positioned is shown in Fig. 4, where $\vec{s}_l$, $\vec{p}_l$, and $\vec{n}_l$ represents the received signal, the original signal, and phase noise, respectively. The PA-LI processing is shown in Fig. 5, and we assume that the number of chirps per frame is $L$, and the phase after accumulation can be written as the follows:

$$\varphi = \arctan\left\{\langle(\vec{p}_l + \vec{n}_l)\rangle\right\}, \quad l = 1, 2, 3 \ldots L, \quad (6)$$

where $\langle \ldots \rangle$ is the ensemble average of the data. Since $\vec{p}$ is essentially constant in a frame period and $\vec{n}$ is small and random, the effect of phase accumulation is that $\vec{p}$ will be amplified numerous times and $\vec{n}$ will cancel each other out, and it is minuscule compared to the accumulated $\vec{p}$. Both the DC offset and the PA methods deal with the signal phase, but the former applies to the entire measurement period or an observation window period, whilst the latter is done frame by frame.

The phase data are unwrapped after phase accumulation to compute the radar vital sign $x(t)$, which can be written as the following formula:

$$x(t) = A_h sin\left(2\pi f_h t\right) + A_b \sin\left(2\pi f_b t\right) + n_c, \quad (7)$$

where $A_h$, $A_b$, $f_h$, and $f_b$ represent the maximal chest displacement caused by heartbeat and breathing, and the frequency of heartbeat and breathing, respectively. $n_c$ refers to the interference of the body's shaking and the clutter. The above parameters vary from person to person. Furthermore, a person's heart rate is not always consistent, and bodily

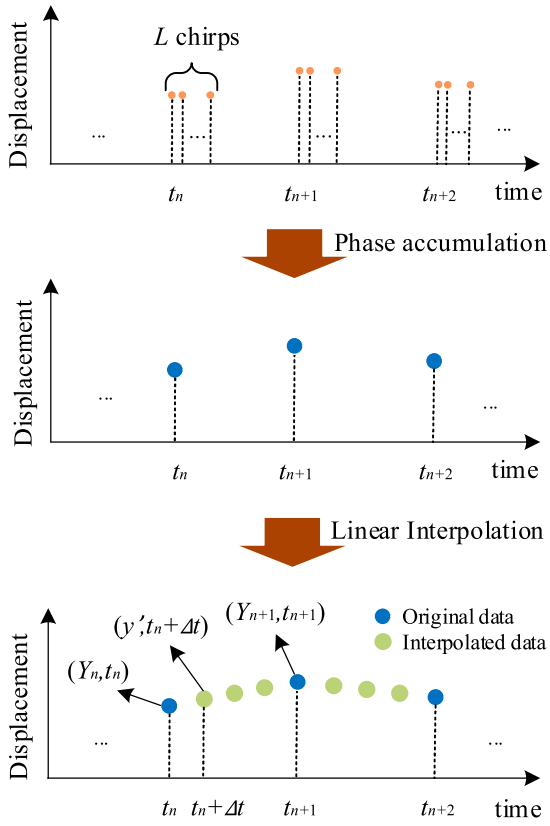


**Fig. 5** Flow chart of PA-LI method.

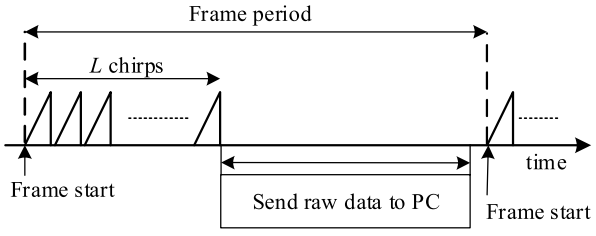


**Fig. 6** Data transmission diagram of the FMCW Radar.

shaking during the measurement is unavoidable. $x(t)$ is thus a non-linear and non-stationary signal.

To extract heartbeat signals with high SNR from $x(t)$, we apply linear interpolation (LI) on the collected $x(t)$ to enhance the sampling rate before performing ICEEMDAN processing because the movement of the chest is quite slow. As shown in Fig. 5, the ordinate value of a certain interpolation point between two adjacent original data is expressed as:

$$y' = Y_n + \Delta t \frac{Y_{n+1} - Y_n}{t_{n+1} - t_n}, \tag{8}$$

where $\Delta t$ is the time elapsed between the interpolation point and the prior original data. The radar vital sign is defined as $X(t)$ after LI processing. For two reasons, this does not contradict the previously indicated phase accumulation.

- First, as shown in Fig. 6, the raw data in each frame period will be kept in the buffer and then sent to the PC once all of the chirps in the frame period have been transmitted. This means that when processing data from several frames directly, the data sampling rate is not consistent.
- Second, due to the time used in data transmission, the frame period in the real experiment should not be shorter than 50 ms (the matching sampling rate cannot be higher than 20 Hz); otherwise, data loss is easily caused.

Our previous work [24] indicates that when $L$ is 32 and the sampling rate is 80 Hz, $X(t)$ has a high SNR. Therefore, we chose the optimal settings for this experiment from the above-mentioned.

Following PA-LI processing, we suggest using the ICEEMDAN method to adaptively decompose $X(t)$ into several IMF components and a residual component, followed by separation of the heartbeat signal from noises. The first IMF of $X(t)$ decomposed by EMD is

$$IMF_1(t) = E_1(X(t)) = X(t) - \mathrm{M}(X(t)), \tag{9}$$

where $\mathrm{M}(\ldots)$ is the signal's local mean value and $E_1(\ldots)$ is the signal's first IMF of EMD. It is worth noting that compared to EEMD, ICEEMDAN does not directly add white Gaussian noise. Firstly, break down the white Gaussian noise with EMD, and then add the corresponding decomposed white Gaussian noise while computing the kth IMF of ICEEMDAN. So, the initial signal with noise may be represented as:

$$X^{(i)}(t) = X(t) + \beta_0 E_1\left(w^i(t)\right), \quad i = 1, 2, 3 \ldots I, \tag{10}$$

where $i$ is the number of times that noise is added to the original signal, $\beta_0$ is the noise amplitude coefficient, and $w^i(t)$ is a realization of zero-mean white Gaussian noise. The first IMF of $X(t)$ decomposed using ICEEMDAN is then expressed as follows:

$$IMF_1(t) = \left\langle E_1\left(X^{(i)}(t)\right)\right\rangle = X(t) - \left\langle M\left(X^{(i)}(t)\right)\right\rangle. \tag{11}$$

In summary, the decomposition steps of ICEEMDAN are shown as follows:

1. Using EMD to decompose $X^{(i)}(t)$ to obtain the first residual component and the first IMF.

$$r_1(t) = \left\langle M\left(X^{(i)}(t)\right)\right\rangle, \quad IMF_1(t) = X(t) - r_1(t). \tag{12}$$

2. Calculating the kth residual component.

$$r_k(t) = \left\langle M\left(r_{k-1}(t) + \beta_{k-1} E_k\left(w^i(t)\right)\right)\right\rangle, \quad k = 2, 3, 4 \ldots n, \tag{13}$$

where $E_k$ is the kth IMF decomposed by EMD. $\beta_{k-1}$ is the noise amplitude coefficient of the white Gaussian noise added during the kth decomposition and it is

usually chosen to be 0.1–0.3 [32].

3. Calculating the kth IMF.

$$IMF_k(t) = r_{k-1}(t) - r_k(t). \tag{14}$$

4. Repeat step 2 and 3 until a total of $n$ IMFs and a residual component $r_n$ are obtained, and the original signal can be illustrated by:

$$X(t) = \sum_{k=1}^{n} IMF_k(t) + r_n(t), \quad k = 1, 2, 3 \ldots n. \tag{15}$$

After decomposing $X(t)$ with ICEEMDAN, we perform FFT spectrum analysis on all IMFs.

Under typical conditions, the volunteer's heart rate changes are not substantial during a single observation window cycle; therefore, the heartbeat signal is more concentrated in energy on the spectrum and has a single peak. Furthermore, the ICEEMDAN technique successfully solves the mode mixing problem, enabling the heartbeat signal to be decomposed into a single IMF. Even if an IMF is formed in the 0.8–2.0 Hz range by noise, mode mixing, and spurious modes, its SNR will be lower than the real heart IMF with a single peak. Therefore, the IMFs of peak frequency at 0.8–2.0 Hz are selected by the IMF filter, and the one with the highest SNR is the heart IMF for the heartbeat signal reconstruction. In addition, if no IMF whose peaks in this range or the SNR of the heart IMF from several consecutive observation windows is low, it is considered an abnormality. The system will output the IMF closest to the regular heart rate band as a result. This situation is extremely uncommon, and we believe that it will only occur when the subjects have an abnormal heart rate. Therefore, when the proposed heart rate measurement system is employed in actual medical monitoring, the SNR threshold of heart IMF will be set, and an alarm is sent if an abnormal condition arises.

## 4. Our Experiment

### 4.1 Experimental Method

Our experiments employed an FMCW radar module based on a Texas Instruments IWR1443 chip with an operational frequency range of 77 to 81 GHz. The maximum effective isotropic radiated power (EIRP) is 21 dBm, which complies with FCC regulations and will not hurt the human body. Besides, the radar module is allowed to be used according to the Japanese Radio Law. The parameters of the radar module are shown in Table 1.

Four of our volunteers (A height: 166 cm, weight: 60 kg; B height: 179 cm, weight: 64 kg; C height: 177 cm, weight: 75 kg; D height: 173 cm, weight: 60 kg) maintained a standing position during the heart rate measurements. As indicated in Table 2 and Fig. 7, the radar module was successively positioned in different places to investigate the influence of different measurement orientations on heart rate

**Table 1** Radar parameters.

| Parameters | Value |
|---|---|
| Bandwidth | 3.99 GHz |
| Sweep time | 57 μs |
| Frame period | 100 ms |
| Slope | 70 MHz/μs |

**Table 2** Radar position.

| Position | Elevation angle [°] | Distance [m] |
|---|---|---|
| Front | 0 | 1 |
| Front | 0 | 1.5 |
| Front | 0 | 2 |
| Front | 30 | 1.5 |
| Front | 60 | 1.5 |
| Front (Top) | 90 | 1.3-1.5 |
| Back | 0 | 1 |
| Left | 0 | 1 |
| Right | 0 | 1 |

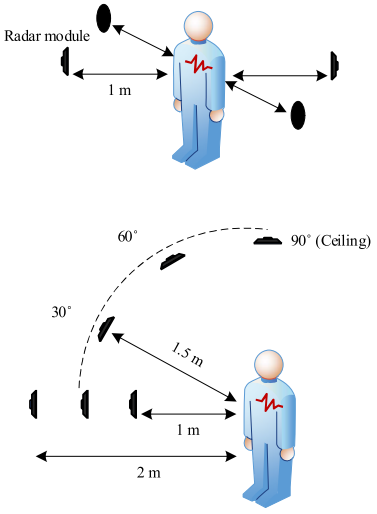


**Fig. 7** A radar module was placed at 9 different positions for heart rate measurements, and only one volunteer was measured at the same time.

estimates. First, we measured one meter in front of the radar module and compared the findings to previous studies to demonstrate the reliability of our proposed method. Secondly, we take measurements through the radar module placed in front, behind, left, and right of the volunteers (distance: 1 m) and compare the results with and without PA-LI method to demonstrate PA-LI's validity discussed in paper [24]. Next, the elevation angle between the volunteer and the radar module was held at 0 degrees. Its effect on the accuracy of the proposed method's heart rate measurements was tested by varying the distance between them (1 m, 1.5 m, 2 m). Finally, since the distance from the ceiling to the shoulder is about 1.5 m when a person is standing, we kept the distance between the radar module and the volunteer at 1.5 m. We varied the elevation angle between them (0°, 30°, 60°, 90°) to observe the effect of its variation on heart rate estimation. Some of the experimental scenarios are shown in Fig. 8.

To obtain an accurate reference heartbeat signal, the volunteers wore an electrocardiogram (ECG) device during

**(a)** Experimental scenario 1 (Distance: 1.5 m; Elevation angle: 60°).

**(b)** Experimental scenario 2 (Distance: about 1.5 m; Elevation angle: 90°).

**Fig. 8** In (a) and (b), the radar module is fixed by a tripod or affixed to the ceiling, respectively. In (b), the distance between the radar module and the volunteer is kept at about 1.5 m, although it varies from person to person.

the measurement time of 60 s. Then, 60 s streaming data is analyzed with a 15 s observation window and a 1 s sliding step. Next, calculate each observation window's heart rate and compare it with the ECG data to obtain the root mean square error (RMSE). The definition of RMSE is shown in the following formula:

$$\mathrm{RMSE} = \sqrt{\frac{1}{P}\sum_{P=1}^{P}\left(y_p - o_p\right)^2}, \quad p = 1, 2, 3 \ldots P, \quad (16)$$

where $P$, $y_p$, and $o_p$ are the number of observation windows, the heart rate measured by each observation window, and the reference heart rate, respectively. In this paper, the definition of SNR is as follows:

$$\mathrm{SNR} = 10\log\left(\frac{s^2(l)}{\sum s^2(f) - s^2(l)}\right), \quad (17)$$

where $f$ and $l$ are the index number corresponding to each frequency component and the peak of the signal spectrum, respectively. Therefore, $s^2(l)$ means the peak value of the signal spectrum and $\sum s^2(f)$ is the total energy of the signal spectrum.

### 4.2 Experimental Results

The heart IMFs obtained by ICEEMDAN decomposition of the radar vital sign processed by PA-LI or without PA-LI are shown in Fig. 9. The findings reveal that the heart rates determined by ECG data, traditional ICEEMDAN, and the

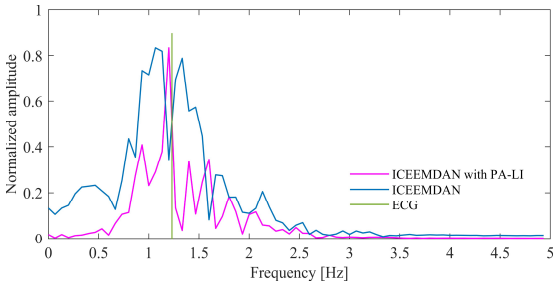


**Fig. 9** The frequency spectrum of ICEEMDAN heart IMF of a certain observation window with or without PA-LI processing is shown in this figure.

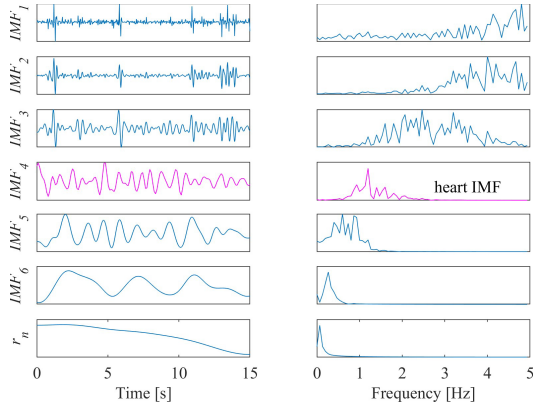


**Fig. 10** The results of ICEEMDAN processing of the radar vital sign (measured from the front 1 m). The time-domain waveforms of each IMF and the final residual are shown on the left, and their corresponding frequency-domain is shown on the right.

proposed method were 1.230 Hz, 1.200 Hz, and 1.067 Hz, respectively, with the accuracy of the two methods being around 86.7 percent and 97.7 percent. The suggested method's accuracy was 11.0 percent greater than the comparative method's. Since sometimes the heart IMF decomposed by the conventional ICEEMDAN method does not necessarily have a high SNR, it will be difficult to find the peak and estimate the heart rate. Instead, PA-LI can effectively increase the SNR of ICEEMDAN heart IMF and make it more accurate to find the heart IMF spectrum's peak value. This is because the PA-LI method eliminates phase noise and increases the data length within a certain period of time to improve the SNR of the original signal.

We can also analyze the signal with a 15-second observation window rather than the 20-second observation window of [23], which improves system performance in real-time. The results of the ICEEMDAN decomposition of a certain observation window after the radar vital sign acquired by the proposed method are presented in Fig. 10. The peak frequency of $\mathrm{IMF}_4$ (pink line) is within 0.8–2.0 Hz. In addition, as shown in Fig. 10, $\mathrm{IMF}_4$ exhibits a high degree of consistency with the ECG signal in this observation window. Therefore, $\mathrm{IMF}_4$ is the heart IMF of this observation window, and we utilize it to reconstruct the heartbeat signal.

The comparison of the reconstructed heartbeat signal

**Table 3** Heart rate estimation results at 1 m from the radar module (RMSE: [bpm], SNR: [dB]).

| Subject | Front | | | | Back | | | | Left | | | | Right | | | |
|---|---|---|---|---|---|---|---|---|---|---|---|---|---|---|---|---|
| | Without PA-LI | | With PA-LI | | Without PA-LI | | With PA-LI | | Without PA-LI | | With PA-LI | | Without PA-LI | | With PA-LI | |
| | RMSE | SNR | RMSE | SNR | RMSE | SNR | RMSE | SNR | RMSE | SNR | RMSE | SNR | RMSE | SNR | RMSE | SNR |
| A | 5.69 | -12.98 | 4.09 | -8.27 | 8.14 | -10.15 | 5.95 | -7.16 | 10.80 | -13.44 | 5.90 | -12.91 | 15.70 | -5.73 | 19.66 | -5.89 |
| B | 4.60 | -13.12 | 2.61 | -6.00 | 8.79 | -12.70 | 4.60 | -5.00 | 10.09 | -22.87 | 7.77 | -14.36 | 31.60 | -17.43 | 21.67 | -10.08 |
| C | 4.27 | -15.06 | 2.59 | -7.05 | 10.52 | -12.29 | 7.30 | -7.04 | 8.84 | -17.32 | 6.02 | -14.01 | 26.71 | -10.37 | 25.55 | -11.56 |
| D | 4.47 | -10.57 | 3.01 | -4.96 | 8.42 | -9.88 | 6.45 | -3.45 | 6.73 | -12.95 | 5.95 | -8.04 | 17.82 | -6.31 | 18.89 | -7.89 |
| Mean | 4.76 | -12.93 | 3.08 | -6.57 | 8.97 | -11.26 | 6.08 | -5.66 | 9.12 | -16.65 | 6.41 | -12.33 | 22.96 | -9.96 | 21.44 | -8.86 |

**Table 4** Heart rate estimation results measured from directly in front of the radar module (RMSE: [bpm], SNR: [dB]).

| Subject | Front 1 m | | Front 1.5 m | | Front 2 m | |
|---|---|---|---|---|---|---|
| | RMSE | SNR | RMSE | SNR | RMSE | SNR |
| A | 4.09 | -8.27 | 4.11 | -9.79 | 5.62 | -10.41 |
| B | 2.61 | -6.00 | 5.69 | -9.00 | 5.96 | -12.48 |
| C | 2.59 | -7.05 | 4.24 | -10.74 | 5.32 | -9.34 |
| D | 3.01 | -4.96 | 5.17 | -12.87 | 5.10 | -11.03 |
| Mean | 3.08 | -6.57 | 4.80 | -10.60 | 5.50 | -10.82 |

**Table 5** Heart rate estimation results measured from the oblique front of the radar module (RMSE: [bpm], SNR: [dB]).

| Subject | 0° | | 30° | | 60° | | 90° (ceiling) | |
|---|---|---|---|---|---|---|---|---|
| | RMSE | SNR | RMSE | SNR | RMSE | SNR | RMSE | SNR |
| A | 4.11 | -9.79 | 6.07 | -13.29 | 6.27 | -10.04 | 8.96 | -11.28 |
| B | 5.69 | -9.00 | 5.11 | -10.69 | 6.21 | -11.59 | 8.54 | -12.73 |
| C | 4.24 | -10.74 | 5.94 | -14.54 | 5.93 | -14.46 | 7.09 | -15.00 |
| D | 5.17 | -12.87 | 5.88 | -14.39 | 5.22 | -13.49 | 7.48 | -15.73 |
| Mean | 4.80 | -10.60 | 5.75 | -13.23 | 5.91 | -12.40 | 8.02 | -13.69 |

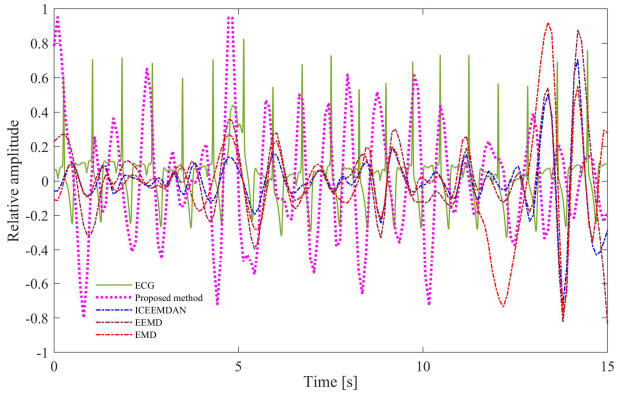


**Fig. 11** Reconstructed heartbeat signals versus ECG waveform in the time domain.

obtained by the EMD, EEMD, ICEEMDAN, and proposed method with ECG data is shown in Fig. 11. For a single observation window, the proposed method and the comparative methods had mean heart rate measurement accuracy of 97.7 percent, 86.7 percent (ICEEMDAN), 81.0 percent (EEMD), and 80.7 percent (EMD), respectively. The bpm (beats per minute) error of the heartbeat signal reconstructed by the proposed method is less than 1. Considering the radar module's own process manufacturing and loss issues may cause a slight measurement error. However, this small error is irresistible and acceptable. Because the RR interval (the time elapsed between two successive R waves of the QRS signal on the electrocardiogram) consistency with the ECG waveform is higher than that of the contrast methods.

The heart rate estimation results for the four directions 1 m away from the radar module are presented in Table 3, where the SNR is averaged over all observation windows. The results show that the mean values of SNR improved by 6.36 dB, 5.60 dB, and 4.32 dB when measured from the "front," the "back," and the "left" using the PA-LI method, and the mean values of RMSE of heart rate measurements decreased by 1.68 bpm, 2.89 bpm, and 2.71 bpm, respectively. This means that the PA-LI effectively improves the SNR and reduces the RMSE of the heart rate measurements. Heart rate was estimated from four directions using the proposed method, with the highest accuracy measured from the "front" and slightly higher accuracy measured from the "back" than the "left." It is noteworthy that the SNR of the heartbeat signal measured from the "back" is the highest among these conditions. This is supposed to be since the back's skin is less displaced, so the effect of breathing on the heart rate measurement is also reduced. However, this also results in heart rate estimates that are not as accurate as those from the "front." Since the skin surface displacement due to the heartbeat is basically not detected from the "right," the accuracy of the measurement from the "right" is not high, and the SNR loses its reference significance.

The heart rate measurements by the proposed method from the "front" direction different distances are shown in Table 4. The average value of the resulting RMSE shows that the measurement accuracy decreases with increasing distance. As the distance to the radar module increases, the SNR of the received signal will decrease, which affects the accuracy of heart rate measurement to some extent. In terms of the individual results, the degree of reduction in measurement accuracy is not absolute. The mean value of the RMSE of heart rate estimation when the distance was 1 m was 3.08 bpm. In [2], their error range of heart rate

measurement of the stationary person was about −7 bpm to 5 bpm in one participant case, proving the reliability of our measurement system. In [1], their average absolute error of heart rate estimation was (2.61, 3.70, 2.12, 3.32, 4.42, mean: 3.23 [bpm]). Our measurement distance is farther than the 0.8 m they measured, and the performance is more stable. The proposed method in the paper [23] had an average RMSE of about 4.45 bpm measured from the front of 1.2 m. Therefore, in all three cases, the accuracy of heart rate measurement was maintained at a high level.

The heart rate estimation results at 1.5 m from the front of the radar module and at different elevation angles are presented in Table 5. Based on the results, it can be seen that the measurement accuracy decreases by about 1 bpm when the elevation angle is slightly increased, and the measurement accuracy does not continue to decrease significantly as the elevation angle increases, and the RMSE remains at about 6 bpm. This is because the relative displacement between the chest and the radar module decreases when the elevation angle increases. When the radar module was fixed to the ceiling, the RMSE was about 8 bpm because the heartbeat produces less shoulder movement than chest movement. Despite this, measurement accuracy, in this case, exceeded the accuracy of heart rate measurements from the "back" and "left" sides based on the conventional ICEEMDAN method.

## 5. Conclusion

In conclusion, we propose a PA-LI joint ICEEMDAN method for mm-wave FMCW radar-based heart rate measurement. The method can address the effects of respiratory signal harmonics, adaptively decompose the radar vital sign to extract the heartbeat signal, and estimate the heart rate. Meanwhile, the PA-LI method can effectively increase the SNR of ICEEMDAN heart IMF and make it more accurate to find the heart IMF spectrum's peak value. Then, the reconstructed heartbeat signal has a high SNR, and the heart rate estimation is more accurate. Besides, we refined previous experimental approaches for investigating the influence of multi-directional observations on heart rate estimates. The experimental results show that the measurements' results in all directions (e.g., left, back, oblique front, and ceiling) are maintained at a high level of accuracy, except for the measurements from the "right" side, because the skin surface displacement (due to the heartbeat) is basically not detected from the "right" side. Considering that non-contact heart rate measurement systems do not always face the subject in practice, in other words, the radar module is installed on the ceiling or high in the room to accommodate the real circumstance. Therefore, our proposed heart rate measurement method has the potential for practical applications.

## Acknowledgments

This research was done with the Graduate School of Science and Technology of Nihon University's financial support. We also thank Mr. Shunsuke Sato and Mr. Ryosuke Koyanaka for their help in collecting experimental data.

## References

[1] C. Ye, K. Toyoda, and T. Ohtsuki, "A stochastic gradient approach for robust heartbeat detection with Doppler radar using time-window-variation technique," IEEE Trans. Biomed. Eng., vol.66, no.6, pp.1730–1741, June 2019.

[2] T. Sakamoto, P.J. Aubry, S. Okumura, H. Taki, T. Sato, and A.G. Yarovoy, "Noncontact measurement of the instantaneous heart rate in a multi-person scenario using X-band array radar and adaptive array processing," IEEE J. Emerg. Sel. Topics in Circuits Syst., vol.8, no.2, pp.280–293, June 2018.

[3] D. Yang, Z. Zhu, and B. Liang, "Vital sign signal extraction method based on permutation entropy and EEMD algorithm for ultra-wideband radar," IEEE Access, vol.7, pp.178879–178890, Dec. 2019.

[4] C. Li, X. Yu, C. Lee, D. Li, L. Ran, and J. Lin, "High-sensitivity software-configurable 5.8-GHz radar sensor receiver chip in 0.13-$\mu$m CMOS for noncontact vital sign detection," IEEE Trans. Microw. Theory Techn., vol.58, no.5, pp.1410–1419, May 2010.

[5] J.C. Lin, "Noninvasive microwave measurement of respiration," Proc. IEEE, vol.63, no.10, pp.1530–1530, Oct. 1975.

[6] B. Park, O. Boric-Lubecke, and V.M. Lubecke, "Arctangent demodulation with DC offset compensation in quadrature Doppler radar receiver systems," IEEE Trans. Microw. Theory Techn., vol.55, no.5, pp.1073–1079, May 2007.

[7] H. Chuang, H. Kuo, F. Lin, T. Huang, C. Kuo, and Y. Ou, "60-GHz millimeter-wave life detection system (MLDS) for noncontact human vital-signal monitoring," IEEE Sensors J., vol.12, no.3, pp.602–609, March 2012.

[8] A. Wiesner, "A multifrequency interferometric CW radar for vital signs detection," IEEE Radar Conference, Pasadena, CA, USA, 2009.

[9] D.T. Petkie, C. Benton, and E. Bryan, "Millimeter wave radar for remote measurement of vital signs," IEEE Radar Conf., Pasadena, CA, USA, 2009.

[10] B. Schleicher, I. Nasr, A. Trasser, and H. Schumacher, "IR-UWB radar demonstrator for ultra-fine movement detection and vital-sign monitoring," IEEE Trans. Microw. Theory Techn., vol.61, no.5, pp.2076–2085, May 2013.

[11] J.C.Y. Lai, Y. Xu, E. Gunawan, E.C. Chua, A. Maskooki, Y.L. Guan, K. Low, C.B. Soh, and C. Poh, "Wireless sensing of human respiratory parameters by low-power ultrawideband impulse radio radar," IEEE Trans. Instrum. Meas., vol.60, no.3, pp.928–938, March 2011.

[12] M. Adjrad, S. Dudley, and M. Ghavami, "Experimental vital signs estimation using commercially available IR-UWB radar," 2014 Int. Radar Conf., Lille, pp.1–4, Oct. 2014.

[13] G. Wang, C. Gu, T. Inoue, and C. Li, "A hybrid FMCW-interferometry radar for indoor precise positioning and versatile life activity monitoring," IEEE Trans. Microw. Theory Techn., vol.62, no.11, pp.2812–2822, Nov. 2014.

[14] G. Wang, J. Muñoz-Ferreras, C. Gu, C. Li, and R. Gómez-García, "Application of linear-frequency-modulated continuous-wave (LFMCW) radars for tracking of vital signs," IEEE Trans. Microw. Theory Techn., vol.62, no.6, pp.1387–1399, June 2014.

[15] D.R. Morgan and M.G. Zierdt, "Novel signal processing techniques for Doppler radar cardiopulmonary sensing," Elsevier Signal Process., vol.89, no.1, pp.45–66, Jan. 2009.

[16] H. Zhao, H. Hong, L. Sun, Y. Li, C. Li, and X. Zhu, "Noncontact physiological dynamics detection using low-power digital-IF Doppler radar," IEEE Trans. Instrum. Meas., vol.66, no.7, pp.1780–1788, July 2017.

[17] S. Sato, Y. Hu, and T. Toda, "A study of multi-directional heart-rate-estimation with discrete wavelet transform and band pass filter with 77 GHz-band FMCW radar," IEICE 1st Int. Conf. on Emerging Technologies for Communs. (ICETC), G1-4, Dec. 2020.

[18] N.E. Huang, Z. Shen, S.R. Long, M.L.C. Wu, H.H. Shih, Q. Zheng,

N.C. Yen, C. Tung, and H.H. Liu, "The empirical mode decomposition and the Hilbert spectrum for nonlinear and non-stationary time series analysis," Proc. R. Soc. Lond. A, vol.454, no.1971, pp.903–995, March 1998.
[19] R. Koyanaka, Y. Hu, and T. Toda, "A study of heart rate estimation with empirical mode decomposition for 77 GHz FMCW radar" IEICE 1st Int. Conf. on Emerging Technologies for Communs. (ICETC), A4-1, Dec. 2020.
[20] Z. Wu and N.E. Huang, "Ensemble empirical mode decomposition: A noise-assisted data analysis method," World Scientific, Advances in Adaptive Data Analysis, vol.1, no.1, pp.1–41, 2009.
[21] M.E. Torres, M.A. Colominas, G. Schlotthauer, and P. Flandrin, "A complete ensemble empirical mode decomposition with adaptive noise," IEEE Int. Conf. on Acoustics, Speech and Signal Processing (ICASSP), Prague, pp.4144–4147, July 2011.
[22] M.A. Colominas, G. Schlotthauer, and M.E. Torres, "Improve complete ensemble EMD: A suitable tool for biomedical signal processing," Elsevier Biomedical Signal Processing and Control, vol.14, pp.19–29, Nov. 2014.
[23] Y. Hu, S. Sato, and T. Toda, "Multi-directional vital signs monitoring on improved complete ensemble empirical mode decomposition with adaptive noise using mm-wave FMCW radar," IEICE 1st Int. Conf. on Emerging Technologies for Communs. (ICETC), A2-5, Dec. 2020.
[24] Y. Hu and T. Toda, "Remote heart-rate estimation based on phase accumulation-linear interpolation method for mm-wave FMCW radar," IEICE Commun. Express., vol.10, no.2, pp.56–61, Feb. 2021.
[25] M. Alizadeh, G. Shaker, J.C.M.D. Almeida, P.P. Morita, and S. Safavi-Naeini, "Remote monitoring of human vital signs using mm-wave FMCW radar," IEEE Access, vol.7, pp.54958–54968, April 2019.
[26] A. Ahmad, J.C. Roh, D. Wang, and A. Dubey, "Vital signs monitoring of multiple people using a FMCW millimeter-wave sensor," IEEE Radar Conference (RadarConf18), Oklahoma City, OK, pp.1450–1455, April 2018.
[27] C. Li, Y. Xiao, and J. Lin, "Experiment and spectral analysis of a low-power $Ka$-band heartbeat detector measuring from four sides of a human body," IEEE Trans. Microw. Theory Techn., vol.54, no.12, pp.4464–4471, Dec. 2006.
[28] S. Wang, A. Pohl, T. Jaeschke, M. Czaplik, M. Köny, S. Leonhardt, and N. Pohl, "A novel ultra-wideband 80 GHz FMCW radar system for contactless monitoring of vital signs," 2015 37th Annual Int. Conf. of the IEEE Engineering in Medicine and Biology Society (EMBC), Milan, Italy, pp.4978–4981, Aug. 2015.
[29] J. Wang, X. Wang, Z. Zhu, J. Huangfu, C. Li, and L. Ran, "1-D microwave imaging of human cardiac motion: An ab-initio investigation," IEEE Trans. Microw. Theory Techn., vol.61, no.5, pp.2101–2107, May 2013.
[30] T. Sakamoto, M. Muragaki, K. Tamura, S. Okumura, T. Sato, K. Mizutani, K. Inoue, T. Fukuda, and H. Sakai, "Measurement of instantaneous heart rate using radar echoes from the human head," Electron. Lett., vol.54, no.14, pp.864–866, 2018.
[31] F. Zhu, K. Wang, and K. Wu, "A fundamental-and-harmonic dual-frequency Doppler radar system for vital signs detection enabling radar movement self-cancellation," IEEE Trans. Microw. Theory Techn., vol.66, no.11, pp.5106–5118, Nov. 2018.
[32] J. Zhang, Y. Guo, Y. Shen, D. Zhao, and M. Li, "Improved CEEMDAN–wavelet transform de-noising method and its application in well logging noise reduction," J. Geophys. Eng., vol.15, no.3, pp.775–787, June 2018.

**Yaokun Hu** received the B.E. degree in electrical engineering and automation from Hunan Institute of Engineering, China, in 2017, and the M.E. degree in electrical engineering from Nihon University, Japan, in 2021, respectively. Since Spring 2021, he is a visiting researcher at the graduate school of science and technology, Nihon University, Japan. He joined Fujitsu Ltd., Japan, in 2021. His current research interests are radar signal processing, biomedical signal processing, and machine learning.

**Takeshi Toda** received a B.E. degree in electrical engineering from Nihon University, Tokyo, Japan in 1992; an M.S. degree in electronic engineering from the University of Electro-Communications, Tokyo, Japan in 1994; and a D.E. degree from the Tokyo Institute of Technology, Tokyo, Japan in 2004. From 1994 to 2004, he worked at Fujitsu Laboratories Ltd., Kawasaki, Japan. From 2004 to 2005, he worked at eAccess Ltd., Tokyo, Japan. From 2005 to 2008, he worked at Kyocera Corp., R&D center, Yokohama, Japan. He is currently a Professor at College of Science & Technology, Nihon University, Tokyo, Japan. His current research interests include radar signal processing, machine leaning, and system information engineering. He is a member of The Institute of Electrical Engineers of Japan.